UNCOVERING DRIVERS OF DISK ASSEMBLY: BULGELESS GALAXIES AND THE STELLAR MASS TULLY-FISHER RELATION

Sarah H. Miller[1,2,3], Mark Sullivan[4,1], & Richard S. Ellis[2]
Draft version November 16, 2012

ABSTRACT

In order to determine what processes govern the assembly history of galaxies with rotating disks, we examine the stellar mass Tully-Fisher relation over a wide range in redshift partitioned according to whether or not galaxies contain a prominent bulge. Using our earlier Keck spectroscopic sample, for which bulge/total parameters are available from analyses of HST images, we find that bulgeless disk galaxies with $z > 0.8$ present a significant offset from the local Tully-Fisher relation whereas, at all redshifts probed, those with significant bulges fall along the local relation. Our results support the suggestion that bulge growth may somehow expedite the maturing of disk galaxies onto the Tully-Fisher relation. We discuss a variety of physical hypotheses that may explain this result in the context of kinematic observations of star-forming galaxies at redshifts $z = 0$ and $z > 2$.

Subject headings: galaxies: evolution — galaxies: fundamental parameters — galaxies: kinematics and dynamics — galaxies: spiral

1. INTRODUCTION

A major goal in galaxy evolution studies is to fundamentally understand the evolving dynamical and morphological forms of galaxies (Roberts 1969). The favored method of tracking the assembly of stellar mass as a fraction of the total mass in rotationally-supported galaxies is the redshift-dependent Tully-Fisher (TF) relation, which was first explored at $z \sim 1$ by Vogt et al. (1996, 1997). Subsequent studies of the stellar mass (M_*)-TF relation at intermediate-to-high redshifts revealed scatters $\sim 3\times$ larger than that of the local relation (e.g., Conselice et al. 2005; Kassin et al. 2007; Vergani et al. 2012). This increased scatter was initially thought to represent a weaker coupling between stellar and dynamical mass, precluding detailed studies of the evolution in either slope or normalization. However, we showed in Miller et al. (2011) and Miller et al. (2012) (hereafter, M11 and M12, respectively) with data of improved signal/noise and refined modeling techniques, that the M_*-TF relation is actually well-established at $z \simeq 1$ with a scatter comparable to that seen in the local relation. Moreover, in M12, we demonstrated that the relation holds for most disk galaxies since $z \simeq 1.7$, thereby posing a challenge of how to explain the rapid evolution in kinematic behavior since $z \sim 2$ where star-forming galaxies are morphologically-irregular and dispersion dominated (Förster Schreiber et al. 2006; Law et al. 2007; Förster Schreiber et al. 2009). To the extent that a TF relation can be examined at $z \simeq 2$ (Cresci et al. 2009; Gnerucci et al. 2011), a normalization increase of 0.4 dex is seen over $\simeq 1$ Gyr to $z \simeq 1.5$, in contrast to only 0.02 ± 0.02 dex over the subsequent 9 Gyr.

Since in M12 the TF scatter is observed to decline by 60% from $z \simeq 1.7$ to $z \simeq 1$, in this present paper we seek to examine whether this might arise from physical properties governing the evolution onto the TF relation. We target our attention on the morphological appearance of each galaxy, specifically the bulge-to-total ratio. Bulgeless disks representing at least 15% of local galaxy populations (Kormendy et al. 2010) provide an interesting challenge for hierarchical ΛCDM galaxy formation (which leads to inevitable bulge-growth without substantial feedback: Robertson et al. 2006; Governato et al. 2010). We test whether the high redshift M_*-TF relation can be better understood when tracking the mature, bulge-dominated population of galaxies separately from the evolving population of bulgeless systems experiencing a more secular formation process.

Throughout the paper we adopt a Chabrier (2003) initial mass function and a $\Omega_\Lambda = 0.7$, $\Omega_m = 0.3$, $H_0 = 70$ km s^{-1} Mpc^{-1} cosmology. All magnitudes refer to those in the AB system (Oke 1974).

2. DYNAMICAL DATA AND STELLAR MASSES

The key measurements required to follow the evolving M_*-TF relations are disk kinematics as parameterized through rotation curve model fits, and stellar mass estimates derived from multi-band photometric data. Our earlier papers (M11, M12) describe the relevant data and their reduction in considerable detail so we provide only a brief summary here.

Our spectroscopic sample was selected from Hubble Space Telescope (HST) Advanced Camera for Surveys (ACS) imaging data in various survey fields complete to an apparent magnitude of i=22.5 and is morphology inclusive, containing irregular and merging systems as well as regular spirals with and without bulges. Keck spectroscopy was undertaken for 236 galaxies with $0.2 < z <$ 1.3 at a median spectral resolution of 30 km s^{-1} using the DEep Imaging Multi-Object Spectrograph(DEIMOS Faber et al. 2003) and, subsequently, 70 $1.0 \lesssim z <$ 1.7 galaxies were targeted at a median resolution of 57 km s^{-1} with the Low Resolution Imaging Spectrograph (LRIS Oke et al. 1995) equipped with a redsensitive CCD. An unique aspect of both spectroscopic

sarah@sarahholmesmiller.com
[1] Department of Physics (Astrophysics), University of Oxford, Keble Road, Oxford, OX1 3RH, UK
[2] California Institute of Technology, Pasadena, CA 91125
[3] University of California, Riverside, CA 92521
[4] School of Physics and Astronomy, University of Southampton, Southampton, SO17 1BJ, UK

campaigns was the use of long exposure times (4-8 hrs) essential for tracking the rotation curves to the flattening radius (see M1 for details). Rotation curves were derived using various emission lines (Hα, [OII], and [OIII] depending on the galaxy redshift. As discussed in M11, we account for position-dependent dispersion and emission brightness profile, convolved with the seeing, and adopt an arctangent function. We use inclination-corrected fiducial velocity measurements at 3.2 times the disk scale radius. The final sample for consideration here comprises 171 galaxies for which rotation curves could be determined (this is all galaxies except for spectrally compact or passive galaxies: see M11 & M12 for details).

Stellar mass estimates are determined using a combination of ground-based K-band infrared imaging, multi-band optical photometry, and spectroscopic redshift information using the spectral energy distribution (SED) fitting technique first utilized by Brinchmann & Ellis (2000). Measured magnitudes in multiple bands were applied using a Bayesian code based on the precepts discussed in Kauffmann et al. (2003), and later Bundy et al. (2005). Using probability distribution functions that incorporate uncertainties in the photometry, the stellar mass uncertainty is better than 0.2 dex for 83% of our sample.

3. MORPHOLOGICAL DATA

Our primary goal is to investigate the possible role bulge formation may play in the apparent rapid evolution of the M_*-TF relation from $z \simeq 2$ to z$\simeq$1. We facilitate this investigation with GALFIT (Peng 2010). As we required disk scale lengths for earlier applications, the bulge-to-disk decomposition procedure described is similar to that in M11, M12, and Miller (2012) and so only briefly discuss the procedure here.

We run GALFIT on each galaxy 1000 times, varying the initial parameters in gaussian distributions based on their SExtractor (Bertin 1996) values. For each object we attempt to fit a deVaucouleurs bulge profile and an exponential disk component, where the fit parameters are the center position, total magnitude $m_{\rm tot}$, effective radius R_e (scale radius, r_s, for an exponential disk), Sérsic index n (fixed to $n = 4$ for deVaucouleurs and $n = 1$ for disk), axis ratio q, and position angle ϕ. Where physical bulge solutions are not found, we re-fit the galaxy with an index-varying single Sérsic component (indices typically lie between $1 < n < 4$). Such cases generally represent disk galaxies which are bulgeless and/or irregular. Disk sizes, inclinations and position angles were taken from best-fit disk components if more than one component was fit. Final parameter uncertainties from the Monte Carlo distributions are better than 5% on average, and we add these uncertainties in quadrature to the photometric errors from GALFIT. The scale radii, position angles and inclinations are typically measured better than 10%. Uncertainties are propagated through to TF parameters, resulting in larger errors for those galaxies which are difficult to constrain.

In the DEIMOS sample, $\sim$40% were adequately fit using a 2-component decomposition, and $\sim$60% benefitted from a single n-varying Sérsic profile fit. In the LRIS sample, the relevant percentages were $\sim$63% and $\sim$37%, respectively. This serves as a good indication of the morphological distribution of our sample; less than half are

well-formed spirals with a clear bulge (§2). Where HST data is available in multiple bands we compared GALFIT runs between bands to test for differences in the scale radius determination as a function of redshift. The scale radii are consistent among the bands indicating no significant redshift-dependent bias (less than 5% in the DEIMOS sample and <10% for that of LRIS). In order to maximize signal/noise we use the GALFIT results from the reddest available filter (F814W or F850LP).

A crucial issue affecting classification at high redshift is the 'morphological k-correction' – the change in apparent morphology with increasing redshift following the drift blue ward in rest-frame wavelength. This is potentially troublesome for $z > 1$ where the the F814W and F850LP images sample the younger star-forming regions rather than the older, redder populations that dominate the stellar mass at lower redshift. As such, there is a danger of underestimating the bulge contribution.

The HST near infrared Wide Field Camera 3 (WFC3/IR) provides a F160W filter, which at $1 < z < 2$ provides rest-frame optical light and is therefore ideal for the bulge-to-disk decompositions we seek. While deep WFC3/IR F160W imaging from the CANDELS survey (Koekemoer et al. 2011) is available for one-fifth of our sample, the majority of the combined LRIS and DEIMOS samples are unfortunately in GOODS North (the WFC3/IR coverage of which will not complete for at least another year). However, for the purposes of this paper we seek only to demonstrate that use of the ACS data to classify the sample broadly into bulge-less and bulge-dominated subsets does not induce significant biases. As we discuss below, we will split our overall sample according to a dividing bulge-to-total ratio (B/T) = 0.1. With this division, we find, for the data with present WFC3/IR coverage, that morphological classifications into these two categories are consistently made between the WFC3/IR and ACS data for 85% of the total sample.

4. RESULTS

We now examine the stellar mass Tully-Fisher (M_*-TF) relation partitioned by morphology, in terms of the bulge/total ratio, B/T. To facilitate this investigation, we separate our sample according to the HST-derived GALFIT results into galaxies with prominent bulges and those without (bulgeless disks and irregulars) as described above. We plot the M_*-TF relation in four redshift bins ($0.2 < z \leq 0.5$, $0.5 < z \leq 0.8$, $0.8 < z \leq 1.2$, $1.2 < z \leq 1.7$) ensuring nearly equal sub-samples and look back time intervals (see Fig. 1). Using the method described in M11, we fit inverse linear regressions to each subsample and z-bin using a fixed slope (of 3.70), the value of which was derived by fitting a free slope to the entire sample. In the two highest redshift bins ($0.8 < z \leq 1.2$, $1.2 < z \leq 1.7$), we see bulgeless disks are significantly offset in the stellar mass (y-axis) normalization from that of the local relation by -0.23 ± 0.06 dex and -0.34 ± 0.07 dex, respectively. In contrast, disks with significant bulges do not deviate significantly from the local relation, nor in fact do bulgeless disks in the two lower redshift bins (Fig. 2). The presence of a bulge appears to secure a disk galaxy on the M_*-TF relation to within a scatter of 0.2 dex.

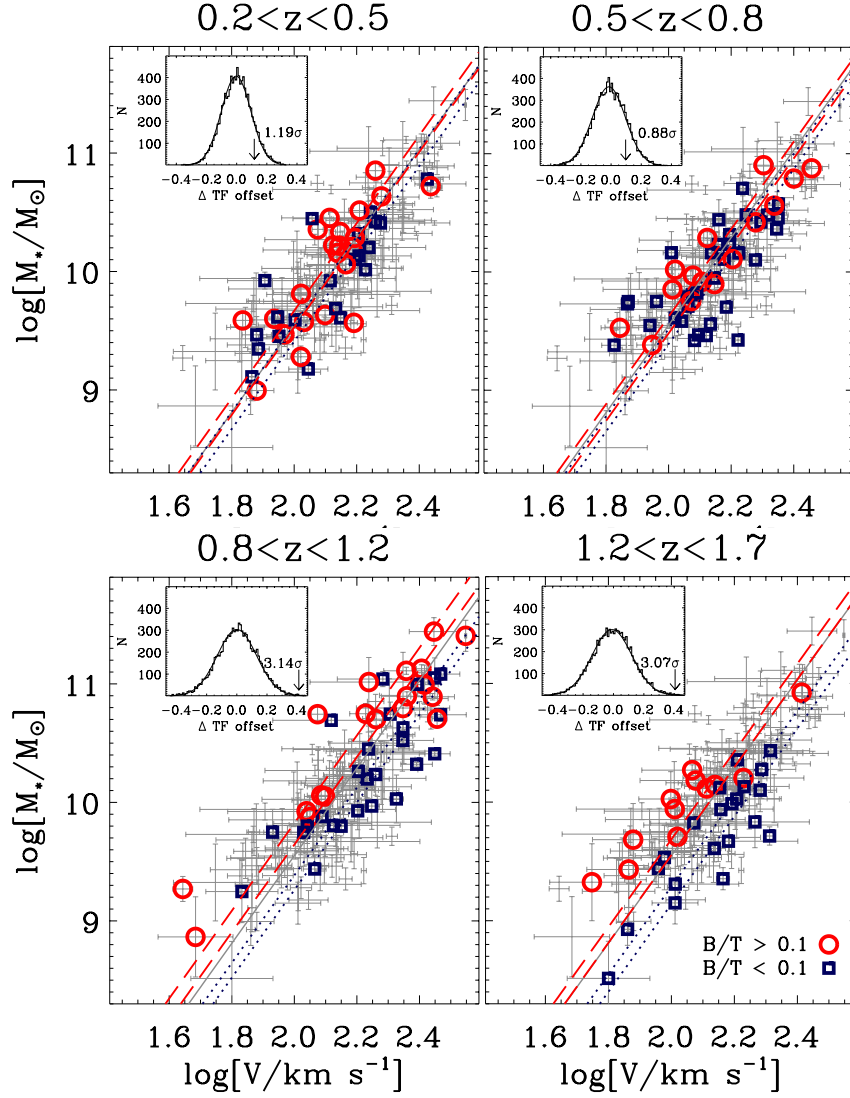The question then arises as to whether increased scat-

FIG. 1.— The M_*-TF relations in four redshift bins. Galaxies with bulges ($B/T > 0.1$) are marked with red circles, and bulgeless/irregular galaxies ($B/T < 0.1$) are marked with navy boxes. The relation of bulge galaxies (red dashed lines, 1-σ) lie along the local relation in each z bin, whereas the bulgeless relation (navy dotted lines, 1-σ) are offset from the local relation in the two highest z-bins. To aid the eye, we plot the total sample with light grey error bars in each panel and include a solid grey line to mark the local relation. To understand the significance of the offsets, a Monte-Carlo 'bootstrap' analysis is conducted for each z-bin, plotted in the inset panels along with the location and significance of the true offset.

ter around the total M_*-TF relation from $z \simeq 1$ to $z \simeq 1.7$ can be accounted for largely via the inclusion of bulgeless galaxies. In M12, the scatter from $z \sim 1$ to $z \simeq 1.7$ increased up to 60%, whereas scatter across the 3 lower bins does not significantly evolve. Since the bulge-separated relations in the highest redshift bins have tighter relations separately than when both samples are combined, it seems likely that increased scatter can be attributed to the zero-point shift of the bulgeless relation. The paucity of lower mass galaxies in the $0.8 < z \leq 1.2$ z-bin arising from the K-band magnitude limit applied for the DEIMOS sample likely complicates this inference (TF scatter increases to lower masses, e.g., Begum et al. 2008). We note that the LRIS sample forming the basis of the highest z-bin was not K-band limited.

To allow for various differences between sample sizes and distributions, we quantify the offset significance for the bulgeless subsample using a Monte Carlo 'boot-strap'

analysis. We fit two TF relations to randomly-selected subsamples ($\times 10,000$, with replacement) of our full data sample (across all redshifts), ensuring subsamples of the same size (N) for each z-bin (N=21/22, 34/15, 26/20, 21/12, for bulgeless/bulge-dominated sets respectively). With each pair of randomly selected subsamples, we measure their relative normalization offset, and fit Gaussians to the resulting histograms of the offset distributions (where the FWHM of each distribution is 0.082, 0.099, 0.086, 0.112 dex for each bin in increasing redshift). We also conduct an additional boot-strap analysis of N=10,000 where we select subsamples at random *within* redshift bins (and also with replacement). This latter method, which accounts for redshift-dependence in the errors, results in broader normalization offset distributions (where FWHMs are 0.098, 0.110, 0.131, 0.132, respectively), and these distributions are plotted in the top left corner of each redshift-bin panel of Fig. 1. The
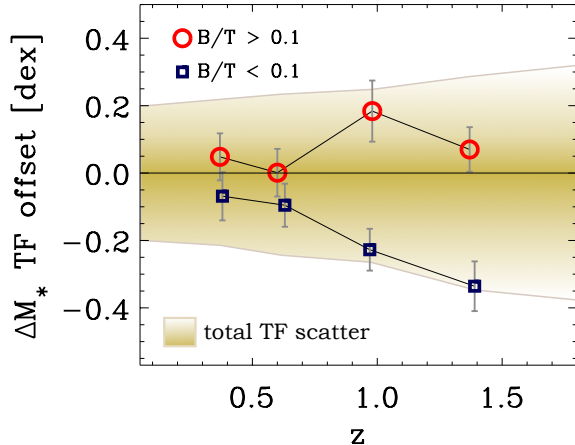
FIG. 2.— Evolution of the relative normalization of the M_*-TF relation, defined as the difference from the local relation (zero-points from fixed-slope fits). Bulgeless galaxies ($B/T<0.1$) are denoted separately from the bulge sample ($B/T>0.1$). We indicate total relation scatter with the gold gradient fill; the offset normalization of the two subsamples occurs within the total scatter of the M_*-TF relation. The bulgeless subsample becomes offset at high-z, but galaxies with bulges do not significantly deviate from the local relation (denoted by the solid black line, ΔM_*-offset = 0.0).

true normalization offset observed in each bin relative to the bootstrapped distribution of the latter method yields offset significances of 1.19σ, 0.88σ, 3.14σ, 3.07σ for each bin in increasing redshift. Together this translates to a confidence interval of greater than 99.8% that the relation of the bulgeless galaxies are offset at high-z due to a genuine effect rather than random error or scatter. The slight decline in significance in the highest bin is due to the reduced number of galaxies with bulges in that bin, even though in real terms the offset of the bulgeless relation is greatest in the highest z-bin (-0.34 ± 0.07).

5. DISCUSSION

In light of our results, we explore explanations of the offset co-evolution of stellar mass and total mass assembly in bulgeless galaxies from those which experienced earlier bulge growth. We first consider in § 5.1 a favored picture in the literature of $z \sim 2$ studies, and then turn in §5.2 and §5.3 to what may be a more self-consistent and simple picture for our results.

5.1. Clump formation and migration

At $z\sim2$, low ratios of rotation-to-dispersion velocity support in disks ($V/\sigma < 2 - 5$, Förster Schreiber et al. 2006, 2009) have been interpreted in a simple picture whereby disks fragment and the resulting clumps migrate to the centers of galaxies to form bulges (Noguchi 1999; Immeli et al. 2004; Romeo et al. 2010).

Importantly, the velocity dispersion measured from such studies comes from the *ionized* gas. The dispersion in the emission lines could be dominated by energy or momentum driven stellar feedback, rather than dispersion from dynamical pressure (as would be traced by the stars and cold gas). In our sample, while there is a spread in V/σ values from 2–15 across all redshift bins (90% never rise above $V/\sigma=10$), no clear trend in σ itself exists with respect to morphology or redshift. These values are more similar to the locally observed spread in V/σ of ionized gas than those found in massive, star-

forming galaxies at $z > 2$ ($0 < V/\sigma < 5$, Genzel et al. 2008).

Furthermore, the clump migration picture does not explain why bulgeless galaxies arrive on the M_*-TF relation by intermediate redshift without forming bulges. In the clump migration picture, gas-rich bulgeless and barless disks would continue to suffer gravitational instabilities and clump formation until a bulge had formed and supposedly stabilized the disk. Some other mechanism is needed to explain the stabilization of bulgeless disks that have yet to form a substantial bulge/bar.

Additionally, central stellar velocity dispersions can support an increased stellar mass in the form of an accumulating bulge without significantly changing the rotational velocity of the surrounding disk. This would shift galaxies above the TF relation as their bulges grow without increasing rotational support, which is not supported by our results.

5.2. An underestimation of gas masses in high-z bulgeless disks

A simpler explanation for our results is that bulgeless galaxies have higher gas fractions in their disks as compared to the rest of the sample. By adding total gas masses to our stellar masses, we may find the baryonic Tully-Fisher is universal at all redshifts in rotationally-supported galaxies. To explore this possibility without direct gas mass measurements, we conduct the following exercise.

We compare the gas estimates from the empirically-based analytical method from M11 (Method 1), to the estimates based on the Kennicutt-Schmidt (K-S) relation (Method 2). Described in detail in M11, Method 1 uses local gas fractions based on a galaxy's stellar mass and self-consistently adds the integrated specific star-formation rate from the galaxy's redshift (accounting for a gas recycling fraction based on the assumed Chabrier IMF). In Method 2, the K-S gas masses are determined from the rest-frame B-magnitude surface brightnesses, which are used to estimate a SFR density and thus a gas mass according to the inverted K-S relation (Kennicutt 1998).

This comparison reveals that the high redshift bulgeless disks have a significantly diminished B-band magnitude per area compared to the rest of the sample. That is to say Method 1 results in 1.11 times more gas than Method 2 with a 10% scatter in bulgeless disks, whereas this factor is 1.43 in the rest of the sample. If we increase the bulgeless disk gas mass estimates 30% so that they align with the rest of the sample, then a universal baryonic TF relation is restored.

Physically, a correction of this nature to our gas mass estimates suggests less metal-enriched gas in bulgeless disks, which is less efficient at forming stars. The relative youth of the bulgeless disks may be due to the lack of enriching outflows re-condensing at $z \sim 1$ (but do by $z \sim 0$). A lengthened 'fountain' duty-cycle could reflect a shallower gravitational potential and lower star-formation surface densities (i.e., Oppenheimer & Davé 2008; Finlator & Davé 2008, etc.), where outflows are slower to re-condense and metals more likely to escape in supernova-driven winds.

Also the simultaneous growth of supermassive black holes (SMBHs) at the centers of galaxies with their bulge

mass is well known(Ferrarese & Merritt 2000). SMBHs are likely fed by gas that has sunk to the centers of galaxies via disk instabilities and/or mergers, a process which would similarly grow a bulge. It is then unsurprising that galaxies with no central bulge may have a much larger fraction of their gas still in their disks.

While the predictions of this exercise await testing via direct gas mass observations, it does suggest interesting implications for a universal baryonic-TF relation (so far confirmed only locally, e.g. McGaugh 2012). Looking towards the future, these predictions can be tested by determining the molecular and neutral hydrogen components of these galaxies, via facilities such as the Atacama Large Millimeter/submillimeter Array (ALMA), or future radio facilities (e.g., MeerKAT, or ultimately the Square Kilometer Array, SKA).

5.3. A z-dependent transition mass

Locally, low-mass bulgeless galaxies ($M_* < 10^9 M_\odot$) tend to fall below the extrapolated M_*-TF relation from $M_* > 10^9 M_\odot$ (Matthews et al. 1998; Stark et al. 2009). Since this offset is similar to that seen in our high-redshift bulgeless galaxies, it suggests that probing further down the stellar-mass function at $0.2 < z < 0.8$ may uncover a similar transition to an offset of bulgeless disks at an intermediate mass between that observed at $z \sim 0$ and at $z > 1$.

The physical significance of an evolving transition mass for bulgeless galaxies could be understood via the 'downsizing' concept (e.g. Cowie et al. 1996) or an evolving 'mass floor' in galaxy formation theory (e.g. Bouché et al. 2010). These models seek to explain why more massive galaxies formed earlier and faster than lower mass galaxies, regardless of environment

(appropriate for our study since the role of environment would be subtle in our field sample). These models are ultimately driven by the cosmic decline in accretion rate, shutting down assembly of massive galaxies first by quickly consuming their reservoirs. A combination of the evolving ultraviolet background with photo-ionizing radiation from the first stars could create a transition mass, above which the cooling efficiency is relatively higher, and below which a lack of self-shielding keeps smaller, thinner disks from remaining neutral (keeping molecular gas collapsing to form GMCs). Galaxies with bulges maintaining thicker disks in thicker, steeper potential-wells could self-shield, and thus form stars more efficiently than thin, bulgeless disks being adversely affected by photo-ionizing radiation in shallower potential-wells.

In attempting to better understand drivers of disk assembly from our results, we note a number of tensions regarding the picture where disks settle from the migration of large clumps into central bulges. Rather, a more self-consistent picture could be provided by an universal baryonic-TF relation, where better accounting of gas in high-z disks could explain the offsets seen in tracking stellar mass with the total rotational support in galaxies. This may also predict a redshift-dependent transition mass which lowers with the age of the universe, below which bulgeless disks assemble their mass offset from the locally-defined M_*-TF relation, but not the baryonic-TF relation.

REFERENCES

Begum, A., Chengalur, J. N., Karachentsev, I. D., et al. 2008, MNRAS, 386, 138
Bertin, E., & Arnouts, S. 1996, A&AS, 117, 393
Bouché, N., Dekel, A., Genzel, R., et al. 2010, ApJ, 718, 1001
Brinchmann, J. & Ellis, R. S. 2000, ApJ, 536, L77
Bruzual, G. & Charlot, S. 2003, MNRAS, 344, 1000
Bundy, K., Ellis, R. S., & Conselice, C. J. 2005, ApJ, 625, 621
Chabrier, G. 2003, PASP, 115, 763
Conselice, C. J., Bundy, K., Ellis, R. S., et al. 2005, ApJ, 628, 160
Cowie, L. L., Songaila, A., Hu, E. M., et al. 1996, AJ, 112, 839
Cresci, G., Hicks, E. K. S., Genzel, R., et al. 2009, ApJ, 697, 115
Faber, S. M., Phillips, A. C., Kibrick, R. I., et al. 2003, SPIE Conference Series, Vol. 4841, ed. M. Iye & A. F. M. Moorwood, 1657–1669
Ferrarese, L. & Merritt, D. 2000, ApJ, 539, L9
Finlator, K. & Davé, R. 2008, MNRAS, 385, 2181
Förster Schreiber, N. M., Genzel, R., Bouché, N., et al. 2009, ApJ, 706, 1364
Förster Schreiber, N. M., Genzel, R., Lehnert, M. D., et al. 2006, ApJ, 645, 1062
Genzel, R., Burkert, A., Bouché, N., et al. 2008, ApJ, 687, 59
Gnerucci, A., Marconi, A., Cresci, G., et al. 2011, A&A, 528, A88+
Governato, F., Brook, C., Mayer, L., et al. 2010, Nature, 463, 203
Immeli, A., Samland, M., Westera, P. et al. O. 2004, ApJ, 611, 20
Kassin, S. A., Weiner, B. J., Faber, S. M., et al. 2007, ApJ, 660, L35
Kauffmann, G., Heckman, T. M., Tremonti, C., et al. 2003, MNRAS, 346, 1055
Kennicutt, Jr., R. C. 1998, ApJ, 498, 541
Koekemoer, A. M., Faber, S. M., Ferguson, H. C., et al. 2011, ApJS, 197, 36

Kormendy, J., Drory, N., Bender, R., et al. 2010, ApJ, 723, 54
Kriek, M., Labbé, I., Conroy, C., et al. 2010, ApJ, 722, L64
Law, D. R., Steidel, C. C., Erb, D. K., et al. 2007, ApJ, 656, 1
Mannucci, F., Cresci, G., Maiolino, R., et al. 2010, MNRAS, 408, 2115
Maraston, C., Daddi, E., Renzini, A., et al. 2006, ApJ, 652, 85
Matthews, L. D., van Driel, W., & Gallagher, III, J. S. 1998, AJ, 116, 2196
McGaugh, S. S. 2012, AJ, 143, 40
Miller, S. H. 2012, PhD thesis, University of Oxford, Astrophysics
Miller, S. H., Bundy, K., Sullivan, et al. 2011, ApJ, 741, 115
Miller, S. H., Ellis, R. S., Sullivan, M. et al. 2012, ApJ, 753, 74
Noguchi, M. 1999, ApJ, 514, 77
Oke, J. B., Cohen, J. G., Carr, M., et al. 1995, PASP, 107, 375
Oppenheimer, B. D. & Davé, R. 2008, MNRAS, 387, 577
Peng, C. 2010, Bulletin of the AAS, Vol. 42, 578–+
Roberts, M. S. 1969, AJ, 74, 859
Robertson, B., Bullock, J. S., Cox, T. J., et al. 2006, ApJ, 645, 986
Romeo, A. B., Burkert, A., & Agertz, O. 2010, MNRAS, 407, 1223
Stark, D. V., McGaugh, S. S., & Swaters, R. A. 2009, AJ, 138, 392
Vergani, D., Epinat, B., Contini, T., et al. 2012, ArXiv e-prints, astro-ph/1202.3107
Vogt, N. P., Forbes, D. A., Phillips, et al. 1996, ApJ, 465, L15+
Vogt, N. P., Phillips, A. C., Faber, S. M., et al. 1997, ApJ, 479, L121+
Zibetti, S., Gallazzi, A., Charlot, S. et al. 2012, ArXiv e-prints